# Nonlinear Oscillations of Black Holes

Huan Yang
Astronomy Department, Tsinghua Universtiy

Collaborators: Neev Khera, Sizheng Ma

IBS-CTPU-CGA QNM & BH Perturbation Workshop，May 27, 2025

# Content

- Classification of linear and nonlinear black hole perturbations.
- Quadratic modes: insights from numerical simulations.
- Quadratic modes: analytical theory.
- Recent progress on QNM tomography.

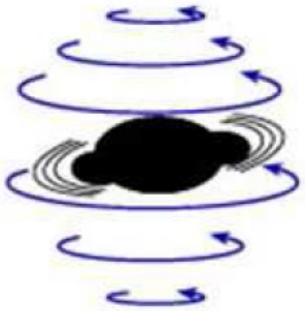

# Content

- Classification of linear and nonlinear black hole perturbations.
- Quadratic modes: insights from numerical simulations.
- Quadratic modes: analytical theory.
- Recent progress on QNM tomography.

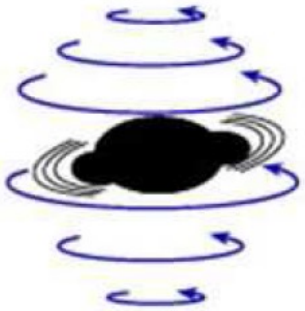

# The simplicity and complexity of BH ringdown

- Black hole spectroscopy targets the QNM spectrum of the final black hole, which has been the main theme of ringdown study in the past decades.

$$h_{RD} \approx \Sigma A_n e^{-i\omega_n t}$$

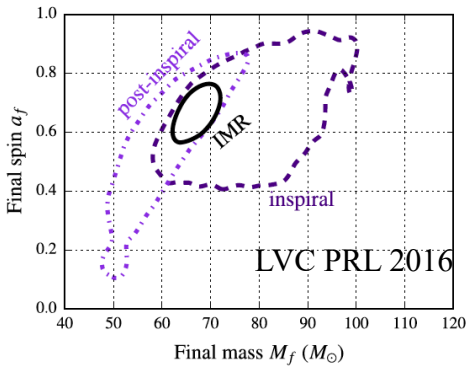

LVC PRL 2016

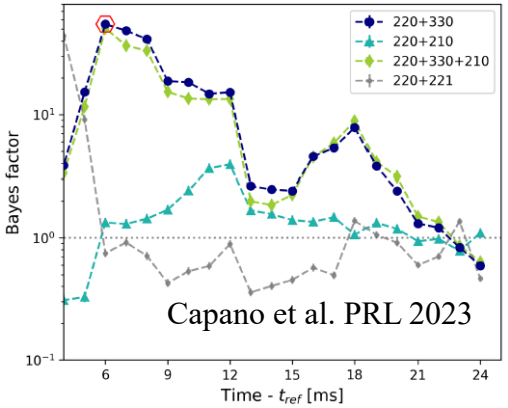

Capano et al. PRL 2023

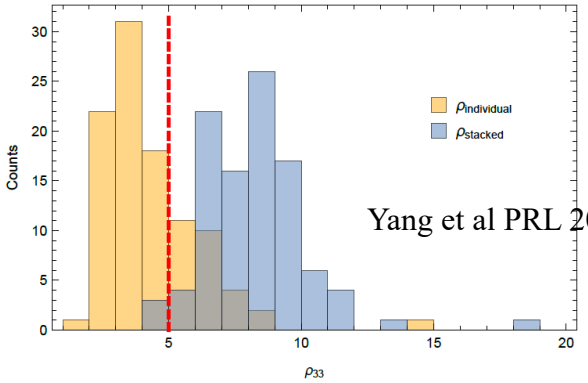

Yang et al PRL 2017

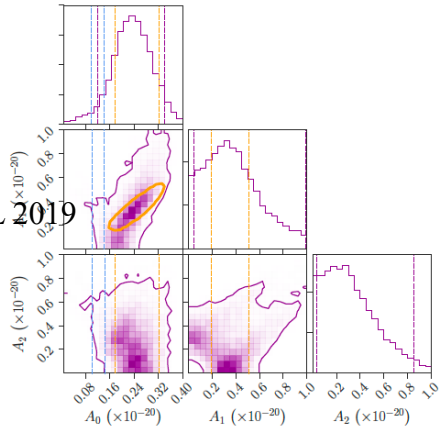

Isi et al. PRL 2019

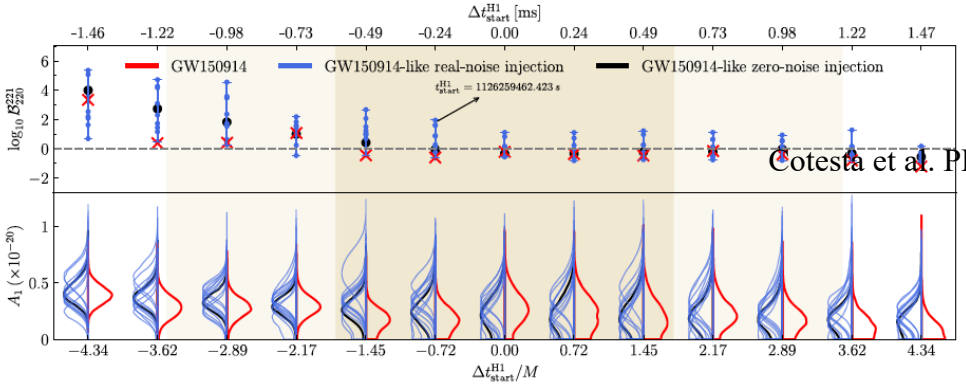

Cotesta et al. PRL 2022

# The simplicity and complexity of BH ringdown

- Black hole spectroscopy targets the QNM spectrum of the final black hole, which has been the main theme of ringdown study in the past decades.
- Ringdown SNR ~O(10) for current detectors, but can be $O(10^2)$ for 3G detectors and LISA.
- From single mode to multiple modes; from mode frequencies to mode amplitudes; from late-time fit to fit-from-the-peak; We are advancing towards non-(linear) mode information of BH ringdown.

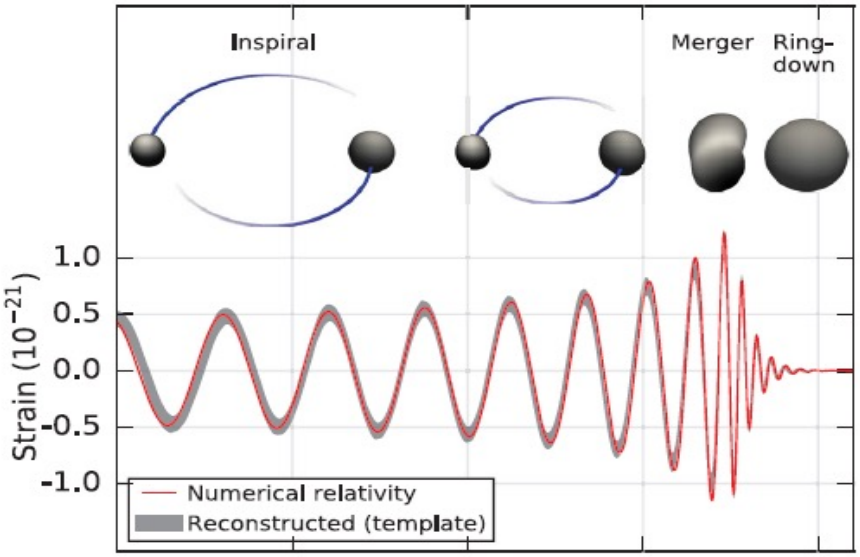

# Beyond black hole spectroscopy

- Various mode and non-modal signals will be measured.
- Beyond black hole spectroscopy: a full ringdown waveform that includes various linear and nonlinear signals may be possible, expressed in mass-ratio expansions.

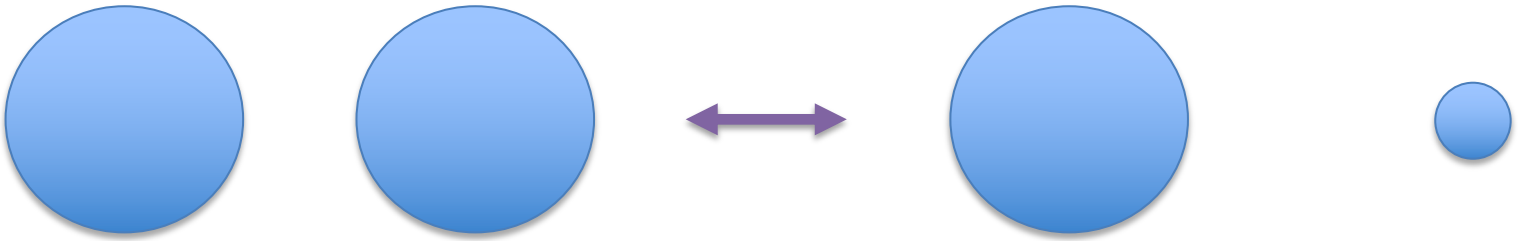

- Theory has to catch up!

$$h = \epsilon h^{(1)} + \epsilon^2 h^{(2)} + \epsilon^3 h^{(3)} + \cdots$$

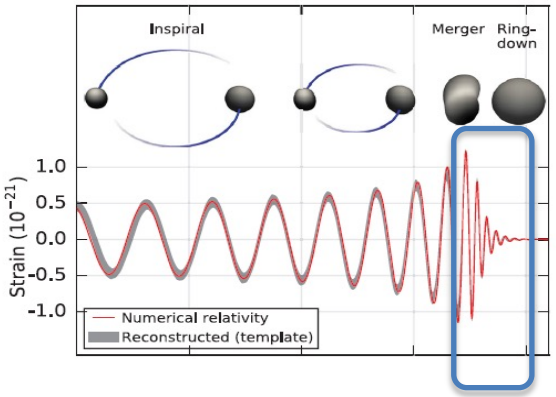

# The decomposition of linear signals

- The linear signal can be decomposed into three parts (Green function): QNMs, Direct part, and tail.

- QNMs are well understood, but the other two parts still requires more quantitative understandings.

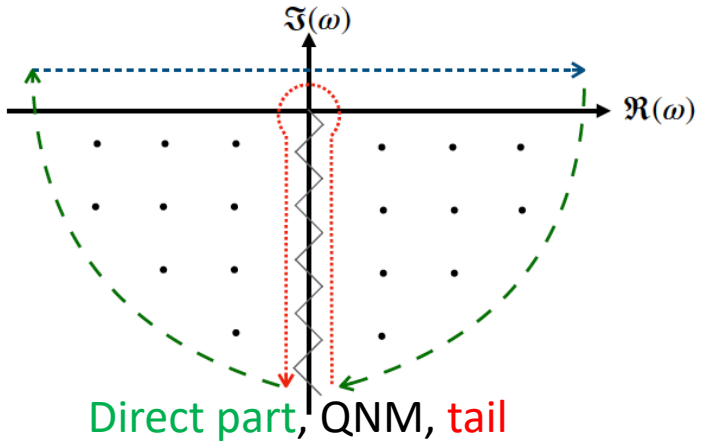


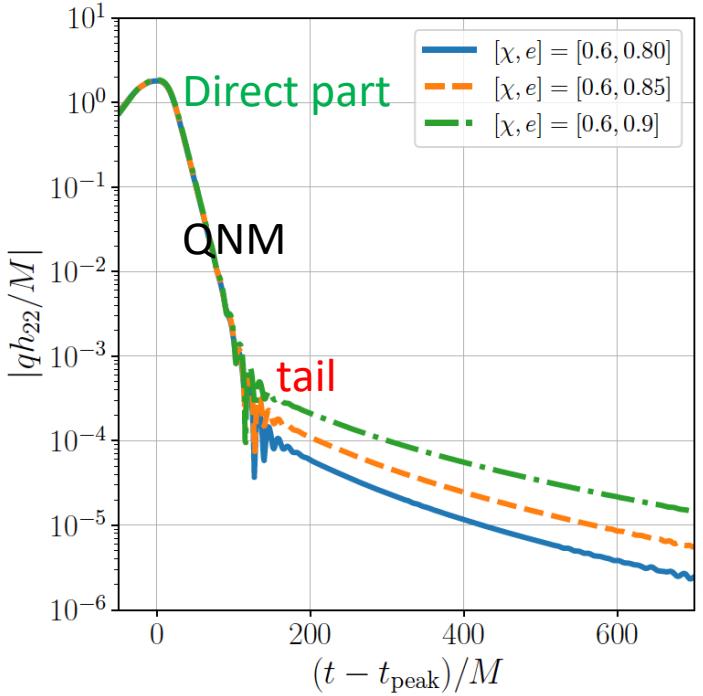

# Classification of nonlinear signals

- The graphic representation of the Green's function:

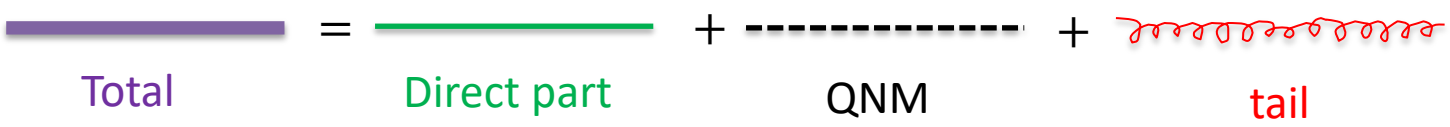


- Second order: mode-mode as the focus of this talk.

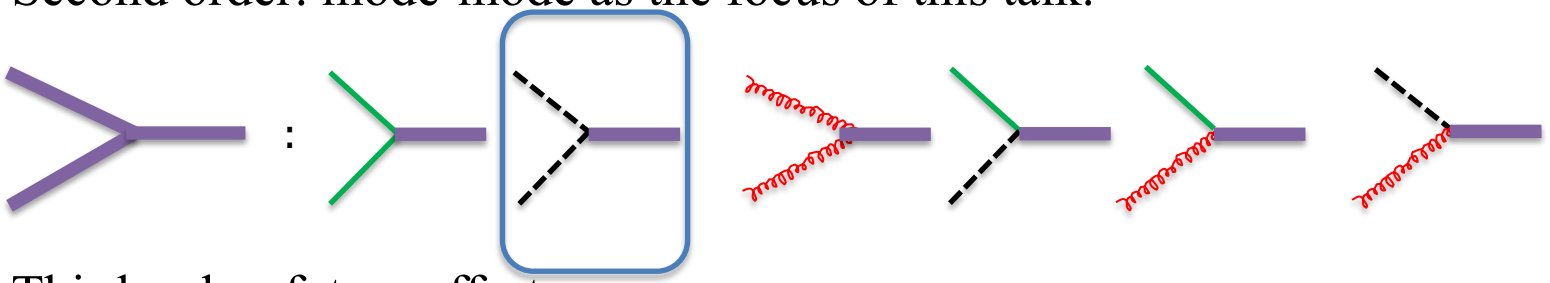


- Third order: future efforts.

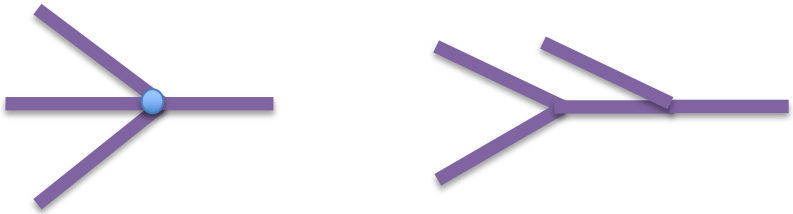

# Content

- Classification of linear and nonlinear black hole perturbations.
- Quadratic modes: insights from numerical simulations.
- Quadratic modes: analytical theory.
- Recent progress on QNM tomography.

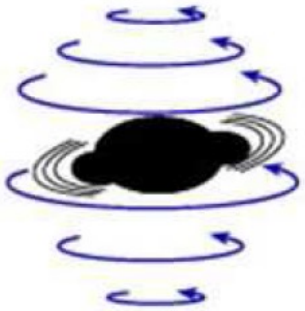

# The early development of 2nd QNM

- Earlier work on second order perturbation of Schwarzschild may be traced back to Gleiser et al in 1996.
- The first calculation on Schwarzschild 2nd order QNM was performed by Nakano and Ioka in 2007 (on the coupling of even-parity modes); later work by [Bucciotti, Juliano,Khagias, Kuntz, Riotto, Trincherini…]

$$\mathrm{O}\,\psi^{(2)} = S(\psi^{(1)}, \psi^{(1)})$$

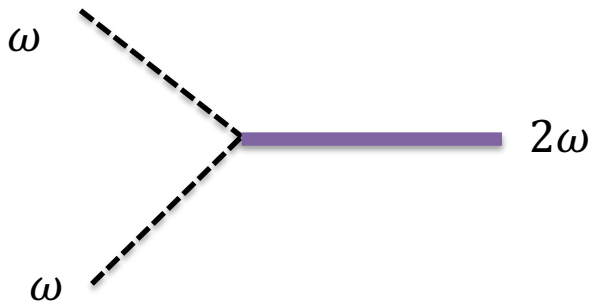


- Quadratic quasinormal mode: mode $(\omega)$ × mode $(\omega)$ → mode $(2\omega)$. The amplitude and phase of the quadratic mode is uniquely determined by the underlying linear mode.

# Quadratic mode at infinity

- Quadratic quasinormal modes are indeed found in numerical simulations [Mitman et al., Cheung et al. PRL 2022]:

- Using linear modes plus additional modes for fitting. Checking the quadratic dependence in amplitudes and check the frequency of the additional mode.

- Spin dependence [Zhu et al.; Redondo-Yuste et al.; Mitman et al …]

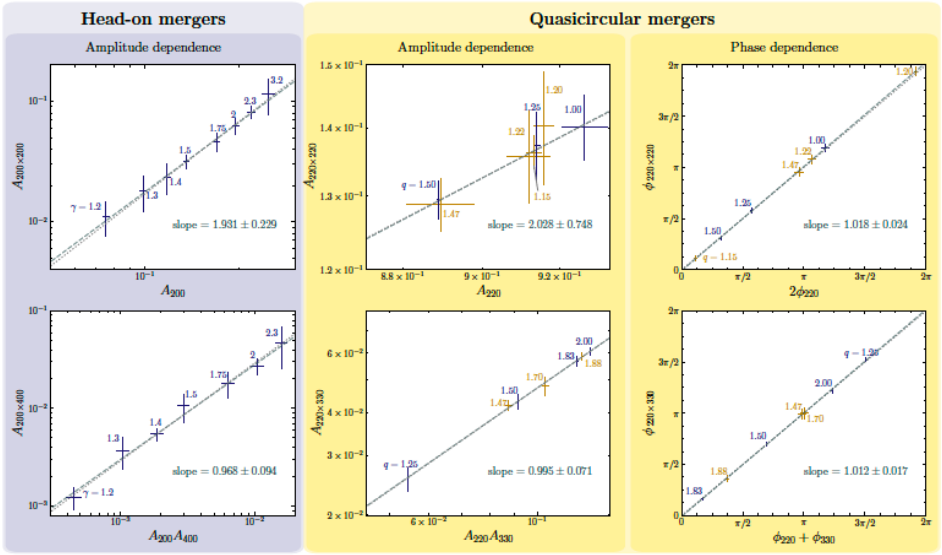


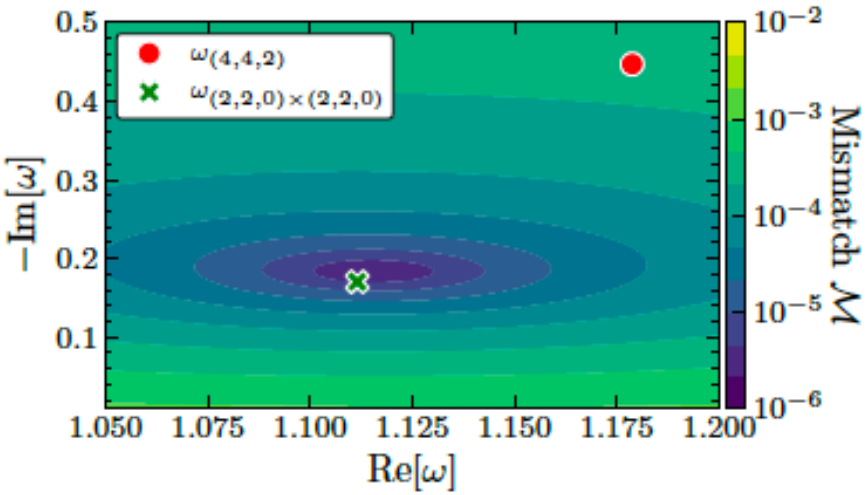

# Quadratic mode on the horizon

- Black hole (isolated) horizon geometry may be described by the shear and other quantities.

$$\sigma(t,\theta,\varphi) = \sum_{l\geq s,m,n,\pm} \mathcal{A}_{lmn} e^{-i\omega^{\pm}_{lmn}(t-t_{\rm rd})+i\phi_{lmn}} {}_2Y_{lm}(\theta,\varphi)$$

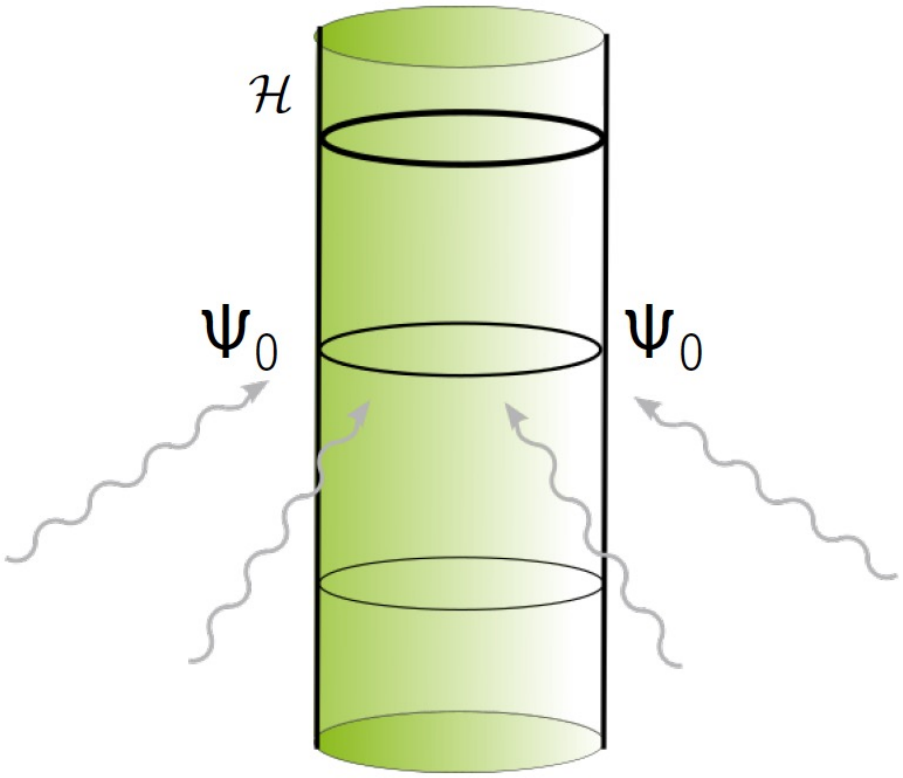


Expansion

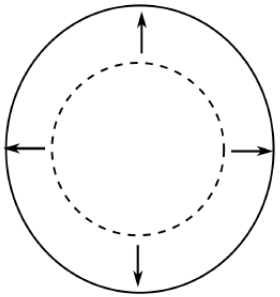

$\Theta_{(\ell)} = 0$

Shear

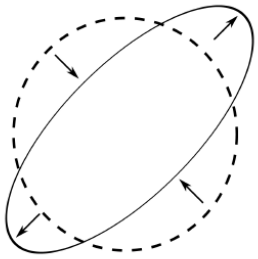

$\sigma \neq 0$

# Quadratic mode on the horizon

- Black hole horizon geometry may be described by the shear and other quantities.

$$\sigma(t,\theta,\varphi) = \sum_{l\geq s,m,n,\pm} \mathcal{A}_{lmn} e^{-i\omega^{\pm}_{lmn}(t-t_{\rm rd})+i\phi_{lmn}} {}_2Y_{lm}(\theta,\varphi)$$

- We have prepared a set of numerical simulations with head-on collisions of non-spinning black holes [Khera,.. HY, PRL 2023].
- We have searched for quadratic modes in the horizon shear and indeed we found them

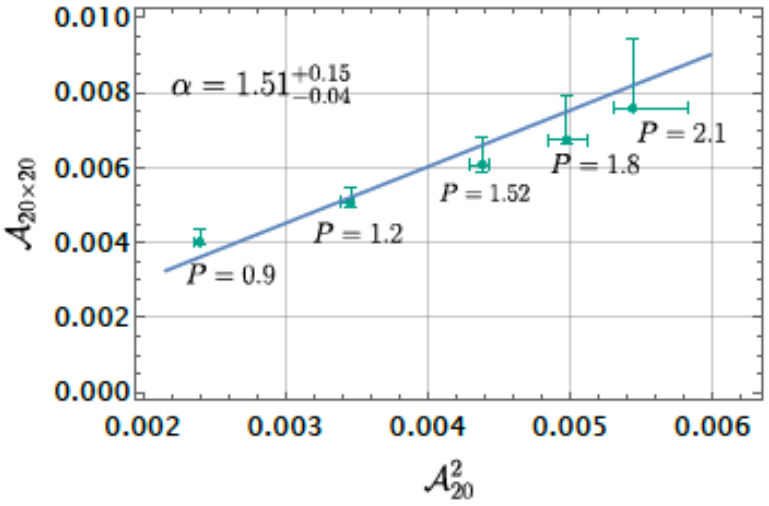


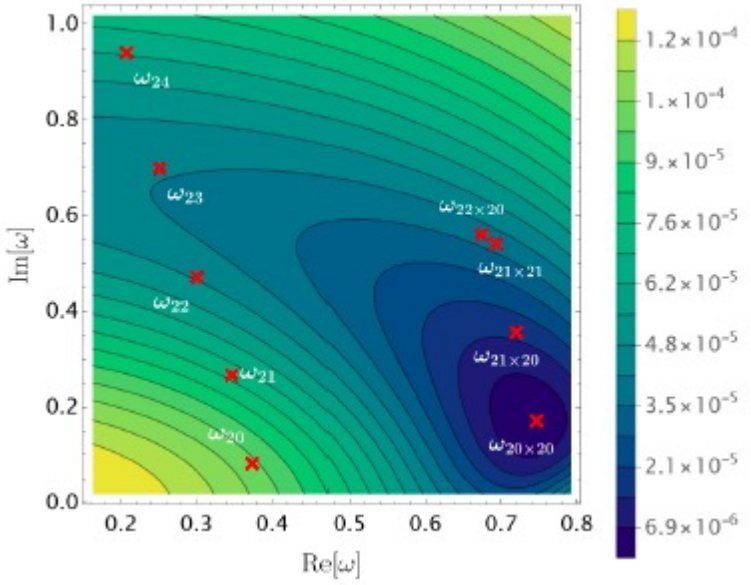

# Quadratic mode fitting

- The evidence of QQNM may be also seen from the mismatch plot: fitting with only modes v.s. fitting with a QQNM.

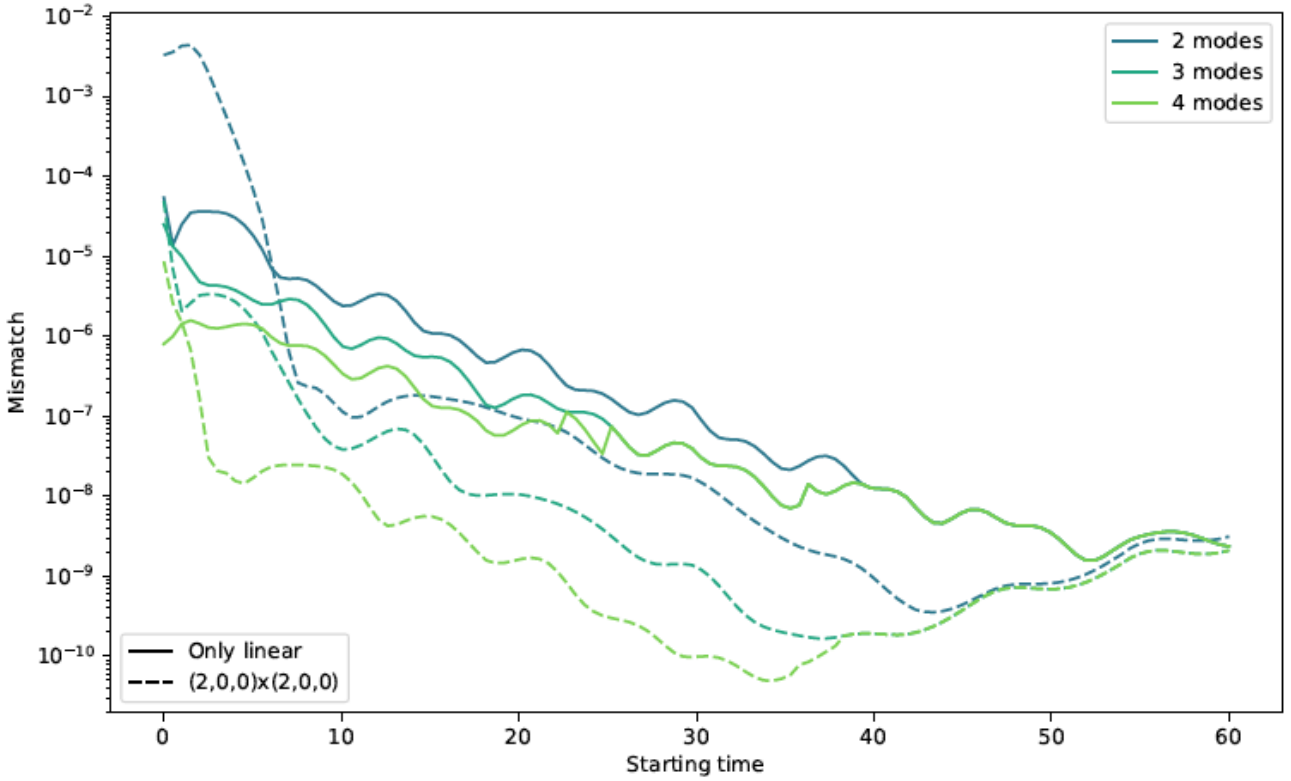

# Content

- Classification of linear and nonlinear black hole perturbations.
- Quadratic modes: insights from numerical simulations.
- Quadratic modes: analytical theory[2401.15516;2410.14529]
- Recent progress on QNM tomography.

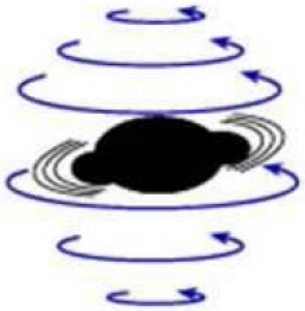

# General Formalism

- Let us consider an expansion of gravitational perturbations of Kerr:

$$\Psi_4 = \epsilon\Psi_4^{(1)} + \epsilon^2\Psi_4^{(2)} + \mathcal{O}(\epsilon^3) \qquad g_{ab} = g_{ab}^{(0)} + \epsilon h_{ab}^{(1)} + \epsilon^2 h_{ab}^{(2)} + \mathcal{O}\left(\epsilon^3\right)$$

- The second order Teukolsky equation may be written as (the source term is a bilinear function on $h^{(1)}$)

$$\mathcal{T}\left[\bar{\Gamma}^4\Psi_4^{(2)}\right] = S_4^{(2)}$$

- Notice that $\Psi$ is complex-valued, but h is real. For any particular QNM, $\Psi$ can have one particular temporal and azimuthal angle dependent term, but h also has its conjugation.

$$\Psi \sim e^{i\omega_{lmn}t}\, e^{im\varphi} \qquad h \sim Ae^{+i\omega_{lmn}t}\, e^{+im\varphi} + A^{*}\, e^{-i\omega_{lmn}^{*}t}\, e^{-im\varphi}$$

# Classification of modes

- Classes of linear modes:
  - $p = \mathrm{sgn}(Re(\omega))$
  - Prograde: $p \times \mathrm{sgn}(m) > 0$; retrograde: $p \times \mathrm{sgn}(m) < 0$
  - Temporal and angular dependence

$$(\mathrm{l,m,n,p}) \rightarrow e^{i\omega^{p}_{lmn}t}\, e^{im\varphi}$$

- The Kerr symmetry implies that

$$\omega^{p}_{\ell mn} = -(\omega^{-p}_{\ell -mn})^{*}$$

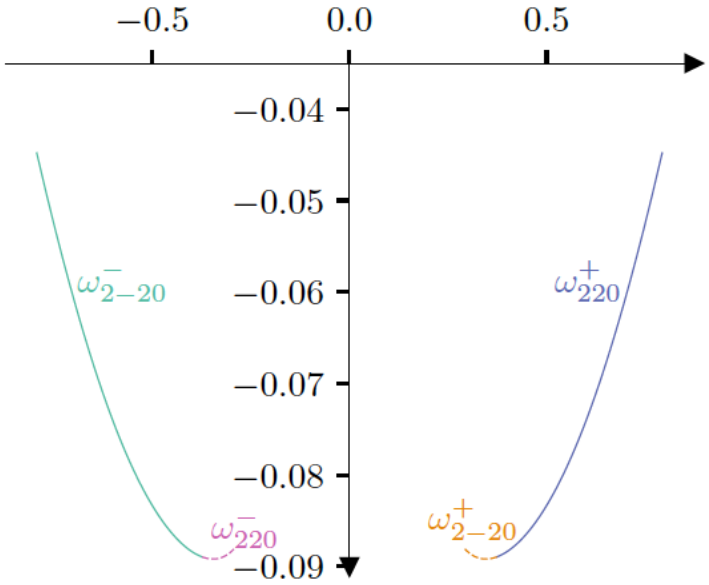


Giesler et al, 2025

# Classification of mode couplings

- Given a QQNM with a certain frequency, what are its parent mode?

$$\begin{pmatrix} \ell_1, & m_1, & n_1, & p_1 \\ \ell_2, & m_2, & n_2, & p_2 \end{pmatrix} \qquad \sim e^{-i(\omega^{p_1}_{\ell_1,m_1,n_1}+\omega^{p_2}_{\ell_2,m_2,n_2})t} e^{i(m_1+m_2)\phi}$$

- There are four possible channels of couplings ($L$,$\bar{L}$):

| | | | |
|---|---|---|---|
| $A_1$ | $(\ell_1, m_1, n_1, p_1)$, | $(\ell_1, -m_1, n_1, -p_1)$, | $A_{-1}$ |
| $A_2$ | $(\ell_2, m_2, n_2, p_2)$, | $(\ell_2, -m_2, n_2, -p_2)$, | $A_{-2}$ |

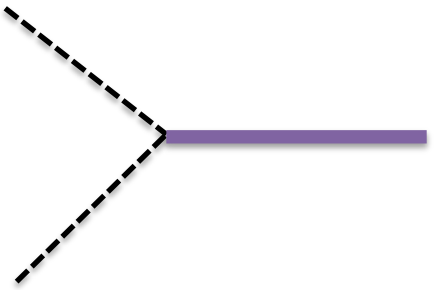

  - $(L_1 \otimes L_2)$: two frequency components $\omega^{p_1}_{l_1 m_1 n_1}$ and $\omega^{p_2}_{l_2 m_2 n_2}$ (++)
  - $(\bar{L}_1 \otimes L_2)$: two frequency components $-\bar{\omega}^{-p_1}_{l_1 -m_1 n_1}$ and $\omega^{p_2}_{l_2 m_2 n_2}$ (-+)
  - $(L_1 \otimes \bar{L}_2)$: two frequency components $\omega^{p_1}_{l_1 m_1 n_1}$ and $-\bar{\omega}^{-p_2}_{l_2 -m_2 n_2}$. (+-)
  - $(\bar{L}_1 \otimes \bar{L}_2)$: zero (--)

# Excitation of a QQNM

- As a result, the QQNM amplitude can be written as

$$A_Q = \mathcal{R}_{++} A_1 A_2 + \mathcal{R}_{+-} A_1 \bar{A}_{-2} + \mathcal{R}_{-+} \bar{A}_{-1} A_2 \,,$$

$$\mathcal{R}^{\rm total} \equiv \frac{A_Q}{A_1 A_2} = \mathcal{R}_{++} + (-1)^{\ell_2} \mathcal{R}_{+-} + (-1)^{\ell_1} \mathcal{R}_{-+}$$ for non-precessional binaries

- For linear modes, ($L$,$\bar{L}$) are mirrors for each other; similarly for QQNM, ($L_1, L_2$) and ($\bar{L}_1, \bar{L}_2$) are mirrors of each other. It can be shown that

$$\mathcal{R}^{(L_1;L_2)}_{c_1 c_2} = (-1)^{\ell_Q + \ell_1 + \ell_2} \bar{\mathcal{R}}^{(\bar{L}_1;\bar{L}_2)}_{c_1 c_2}, \qquad \text{with} \quad c_1, c_2 = (\pm, \pm).$$

- Mode couplings also preserve parities:

$$(\text{even}) \otimes (\text{even}) \to (\text{even}), \quad (\text{odd}) \otimes (\text{odd}) \to (\text{even}), \quad (\text{odd}) \otimes (\text{even}) \to (\text{odd})$$

# Computation method: complex contours

- Coming back to the second order Teukolsky equation:

$$\mathcal{T}\left[\bar{\Gamma}^4\Psi_4^{(2)}\right] = S_4^{(2)}$$

- Consider the solution written as

$$\psi^{(2)} = e^{-2i\omega_L t}e^{2im_L\phi}\sum_l R_l^{(2)}(r)\,S_l^{(2)}(\theta)$$

- The Teukolsky equation may be written as

$$e^{-2i\omega_L t+2im\phi}\sum_l S_l^{(2)}(\theta)$$
$$\times\,(\Delta\mathcal{D}_{-1}^{\dagger\,(2)}\mathcal{D}_0^{(2)} - 12i\omega_L r - \lambda_l^{(2)})R_l^{(2)}(r) = -2\bar{\Gamma}^4\Sigma S_4^{(2)}$$

- $(t, \varphi)$ dependence can be factored out and $\theta$dependence can be removed with projection with spin-weighted spheroidal harmonics.

# Complex contours: eigenvalue perturbation

- A complex contour technique may be applied to deal with divergences of wavefunctions near horizon and infinity.
- This method was previously used to study the eigenvalue perturbation theory [Yang, Zimmerman, Mark, Chen,…]. Imagine an operator equation

$$\mathcal{T}(\omega_0)\psi_0 = 0$$

- If the operator is perturbed:

$$[\mathcal{T}(\omega_0 + \epsilon\omega_1) + \epsilon\Delta\mathcal{T}(\omega_0 + \epsilon\omega_1)]\,(\psi_0 + \epsilon\psi_1) = 0$$

$$\mathcal{T}(\omega_0)\psi_1 + \omega_1\partial_\omega\mathcal{T}\psi_0 + \Delta\mathcal{T}(\omega_0)\psi_0 = 0$$

- The perturbation of eigenvalue is (if the product is self-adjoint)

$$\langle\chi|\mathcal{T}\eta\rangle = \langle\mathcal{T}\chi|\eta\rangle \qquad \omega_1 = -\frac{\langle\psi_0|\Delta\mathcal{T}\psi_0\rangle}{\langle\psi_0|\partial_\omega\mathcal{T}\psi_0\rangle}$$

# Complex contours: eigenvalue perturbation

- This self-adjoint "inner product" or bilinear form may be constructed on a complex contour through

$$\langle\chi|\eta\rangle = \int_{\mathcal{C}} (r-r_+)^s (r-r_-)^s dr \int \sin\theta d\theta\, \chi(r,\theta)\eta(r,\theta)$$

- It has many successful applications [KN QNMs, parametric instability, Chern-Simon QNMs, etc.] Also naturally leads to QNM orthogonality.

$$\mathcal{T}(\omega_a)\psi_a = 0, \mathcal{T}(\omega_b)\psi_b = 0$$

$$\rightarrow \quad \langle\psi_b|\mathcal{T}(\omega_a)\psi_a\rangle = 0, \quad \langle\psi_a|\mathcal{T}(\omega_b)\psi_b\rangle = 0$$

$$\rightarrow \quad \langle\psi_a|(\mathcal{T}(\omega_a) - \mathcal{T}(\omega_b))\psi_b\rangle = 0$$

The same as weight function obtained in Green et al 2022

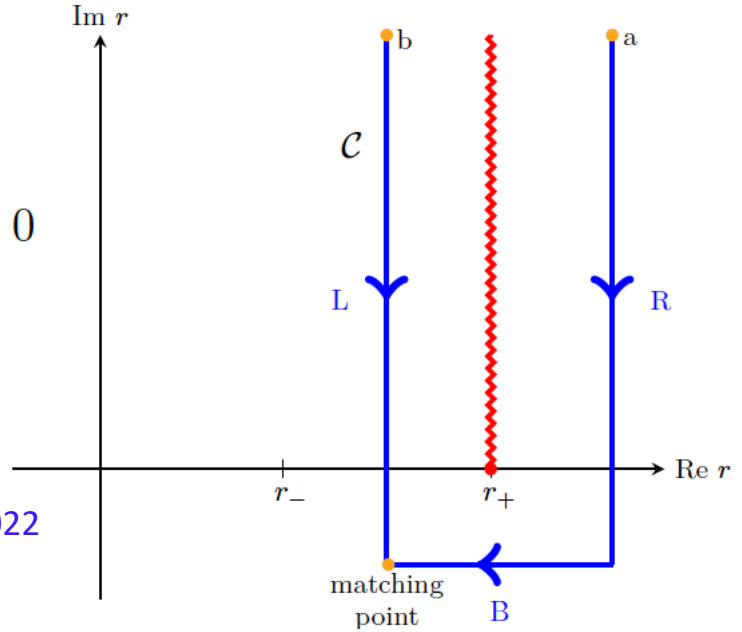

# Complex contours: eigenvalue perturbation

- This self-adjoint "inner product" or bilinear form may be constructed on a complex contour through

$$\langle \chi | \eta \rangle = \int_{\mathcal{C}} (r - r_+)^s (r - r_-)^s dr \int \sin\theta d\theta \, \chi(r,\theta)\eta(r,\theta)$$

- It has many successful applications [KN QNMs, parametric instability, Chern-Simon QNMs, etc.] Also naturally leads to QNM orthogonality.

- In this problem it can be used to compute the wavefunction on the complex contour and obtain the amplitude at infinity through a matching calculation.

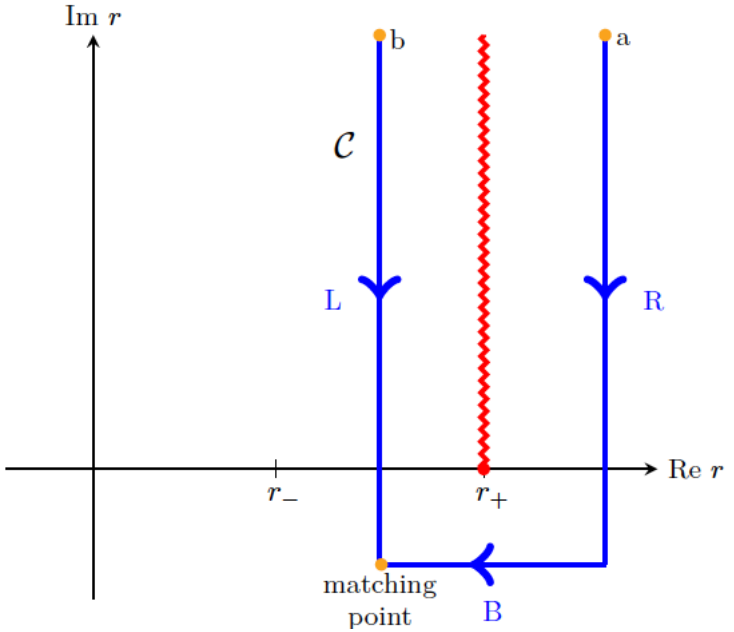

# Computation method: hyperboloidal slicing

- Alternative formulation: consider the expansion of the metric perturbation and the expansion of the Einstein tensor

$$g_{ab} = g^{(0)}_{ab} + \epsilon h^{(1)}_{ab} + \epsilon^2 h^{(2)}_{ab} + \mathcal{O}\left(\epsilon^3\right)$$

$$G_{ab}[g_{ab}] = \epsilon G^{(1)}_{ab}[h^{(1)}_{ab}] + \epsilon^2 G^{(1)}_{ab}[h^{(2)}_{ab}] + \epsilon^2 G^{(2)}_{ab}[h^{(1)}_{ab}, h^{(1)}_{ab}]$$

- At second order we expect

$$G^{(1)}_{ab}[h^{(2)}_{ab}] = -G^{(2)}_{ab}[h^{(1)}_{ab}, h^{(1)}_{ab}]$$

- First order metric perturbation $h^{(1)}$ can be computed from Hertz potential for QNMs in the Outgoing Radiation Gauge

# Computation method: hyperboloidal slicing

- We adopt the hyperboloidal slicing to regularize the wavefunctions and formulate the wave equation [Ripley 2022]. This enables numerical treatment of the reduced Teukolsky equation [Spiers 2022].
- It only gives $\Psi^{(2)}$ that comes from $h^{(2)}$, but in ORG the rest piece is zero.
- We apply the spectral method: quantities are expanded in Chebyshev Polynomials radially and spin-weighted spheroidal harmonics in the angular direction. For example, the Hertz potential is

$$\Phi = R\,\mathcal{R}(R)\,\mathcal{S}(\theta,\Phi)e^{-i\omega T}$$

$$\mathcal{R}(R) = \sum_{n=0}^{\infty} c_n T_n(1-2Rr_+),$$

$$\mathcal{S}(\theta,\Phi) = \sum_{\ell} s_\ell\ {}_2Y_{\ell m}(\theta,\Phi)\,.$$

- At the end the truncated Teukilsky equation turns into a matrix eigenvalue problem.

# Results and comparisons

- For nonprecessing systems the reflection symmetry implies that $A_{-1} = (-1)^{l_1}\overline{A_1}$, which suggests that

$$\mathcal{R}^{\text{total}} \equiv \frac{A_Q}{A_1 A_2} = \mathcal{R}_{++} + (-1)^{\ell_2}\mathcal{R}_{+-} + (-1)^{\ell_1}\mathcal{R}_{-+}$$

- For Schwarzschild black hole $R_{++}$~0.137 (computed with both approaches), $R_{+-}$ ~0.0165, and $R^{\text{total}}$ ~0.1534 $e^{-0.06787i}$,consistent with [Bucciotti et al.]

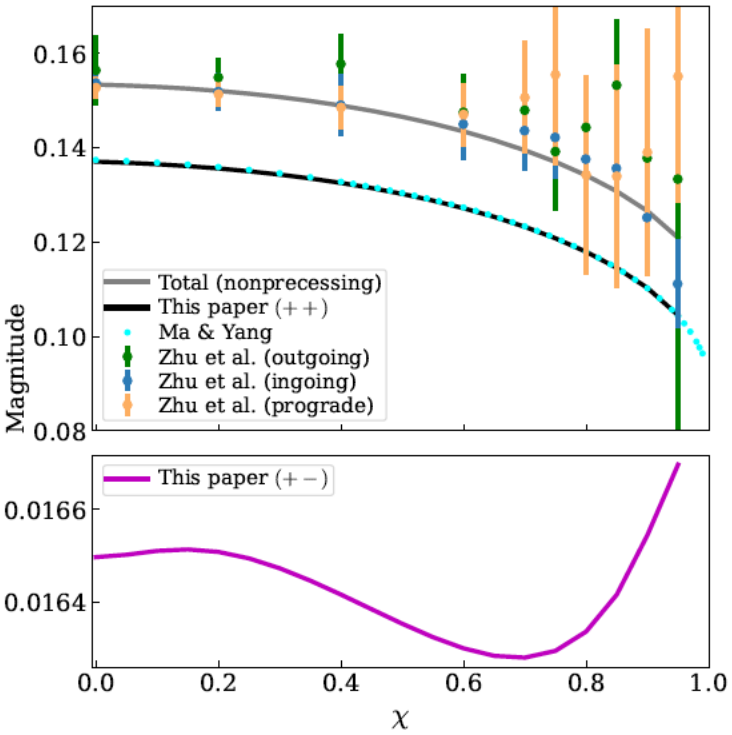


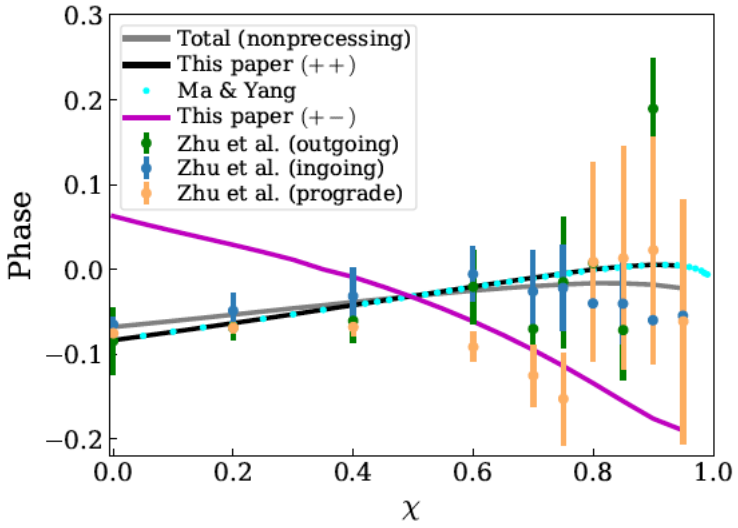

# Results and comparisons

- For nonprecessing systems the reflection symmetry implies that $A_{-1} = (-1)^{l_1}\overline{A_1}$, which suggests that

$$\mathcal{R}^{\text{total}} \equiv \frac{A_Q}{A_1 A_2} = \mathcal{R}_{++} + (-1)^{\ell_2}\mathcal{R}_{+-} + (-1)^{\ell_1}\mathcal{R}_{-+}$$

- For Schwarzschild black hole $R_{++}$~0.137 (computed with both approaches), $R_{+-}$ ~0.0165, and $R^{\text{total}}$ ~0.1534 $e^{-0.06787i}$,consistent with [Bucciotti et al.]

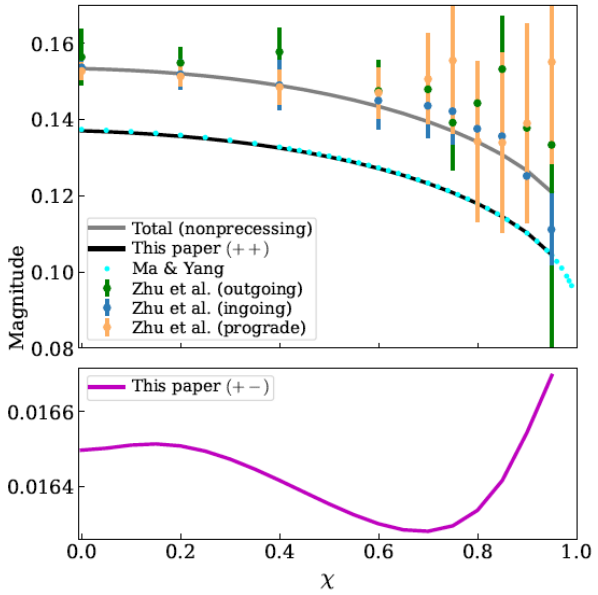


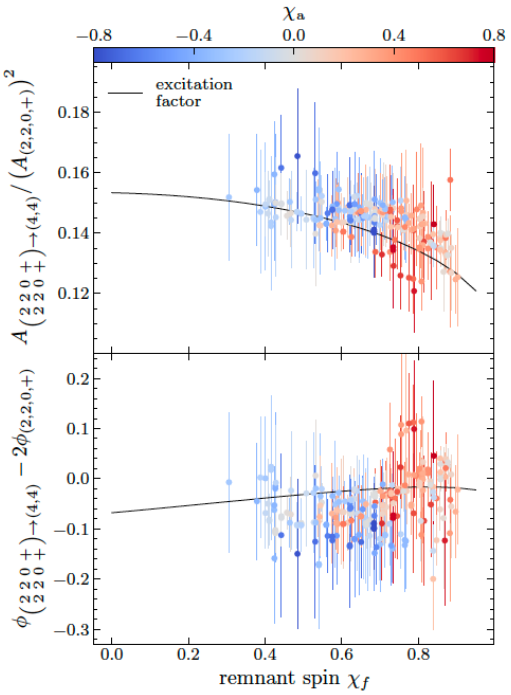


Mitman et al. 2025

# Results and comparisons

- More general mode couplings are considered, where the amplitudes are fitted:

$$R = Ae^{i\phi}, \quad \text{with } A = \sum_{i=0}^{7} A_i \chi^i, \phi = \sum_{i=0}^{7} \phi_i \chi^i$$

- They are summarized in the tables in [Khera et al. PRL 2025], e.g.

| QQNM | Child Harmonic $(\ell, m)$ | Channel | $A_0$ | $A_1$ | $A_2$ | $A_3$ | $A_4$ | $A_5$ | $A_6$ | $A_7$ |
|---|---|---|---|---|---|---|---|---|---|---|
| $\begin{pmatrix}2&2&0&+\\2&2&0&+\end{pmatrix}$ | (4, 4) | $(+,+)$ | 0.1371 | -0.005585 | 0.01943 | -0.2619 | 0.8867 | -1.592 | 1.412 | -0.4997 |
| | | $(+,-)$ | 0.0165 | -0.0001457 | 0.006129 | -0.04495 | 0.1308 | -0.1975 | 0.1517 | -0.04564 |
| $\begin{pmatrix}3&3&0&+\\2&2&0&+\end{pmatrix}$ | (5, 5) | $(+,+)$ | 0.3608 | 0.02932 | 0.07302 | -0.8313 | 2.784 | -4.999 | 4.432 | -1.568 |
| | | $(+,-)$ | 0.05032 | 0.003027 | 0.01122 | -0.1226 | 0.4119 | -0.7302 | 0.6395 | -0.2213 |
| | | $(+,-)$ | 0.009198 | 0.001532 | -0.0002162 | 0.003541 | -0.0189 | 0.04243 | -0.04322 | 0.01752 |
| $\begin{pmatrix}4&4&0&+\\2&-2&0&-\end{pmatrix}$ | (2, 2) | $(+,+)$ | 0.0289 | 0.01489 | 0.0405 | -0.3652 | 1.065 | -1.568 | 1.171 | -0.3534 |
| | | $(+,-)$ | 0.4171 | 0.01512 | 0.05565 | -0.5754 | 1.934 | -3.438 | 3.019 | -1.052 |
| | | $(-,+)$ | 0.01829 | 0.02588 | -0.06939 | 0.05871 | 0.1518 | -0.3899 | 0.3364 | -0.101 |
| $\begin{pmatrix}2&2&0&+\\2&0&0&+\end{pmatrix}$ | (2, 2) | $(+,+)$ | 0.05129 | 0.002777 | -0.03533 | 0.2996 | -1.03 | 1.837 | -1.623 | 0.569 |
| | | $(+,-)$ | 0.002267 | 0.007251 | -0.04791 | 0.3853 | -1.324 | 2.365 | -2.092 | 0.7351 |
| | | $(-,+)$ | 0.002277 | -0.002326 | -0.0002231 | 0.002508 | -0.00836 | 0.01393 | -0.01062 | 0.002952 |
| $\begin{pmatrix}3&3&0&+\\2&-2&0&-\end{pmatrix}$ | (2, 1) | $(+,+)$ | 1.554 | -12.84 | 50.72 | -123.4 | 195.0 | -193.3 | 108.1 | -25.79 |
| | | $(+,-)$ | 0.1214 | -0.07163 | -0.7033 | 5.926 | -18.9 | 29.89 | -23.39 | 7.367 |
| | | $(-,+)$ | 1.359 | -11.42 | 44.2 | -99.21 | 142.2 | -130.1 | 69.21 | -16.1 |

TABLE I. Polynomial fit coefficients for the magnitude of $R$. Spin-weighted spherical harmonics are used as the angular basis.

# Future detectability

- With the theoretical mode couplings we forecast the detectability of various $2^{nd}$ order QNMs for $3^{rd}$ generation ground-based detector and LISA.

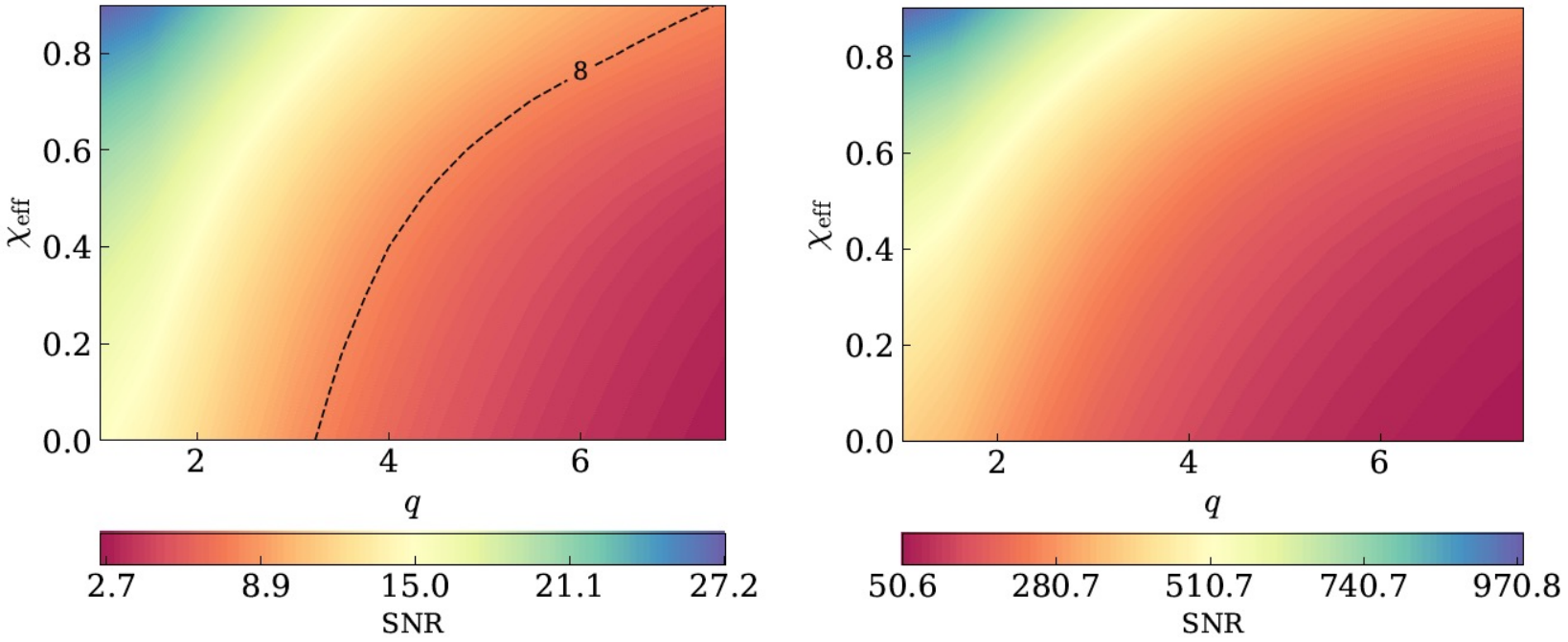


FIG. 6. The SNR of $\begin{pmatrix} 2, & 2, & 0, & + \\ 2, & 2, & 0, & + \end{pmatrix}$, assuming CE (left) and LISA (right).

# Future detectability

- More modes will be detected by CE (even more for LISA):

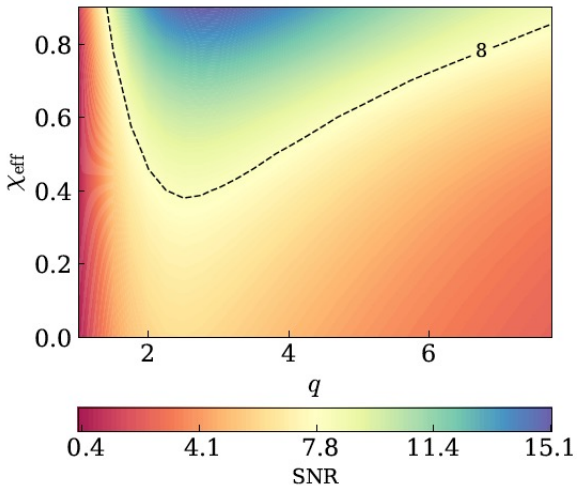


$$\begin{pmatrix} 3, & 3, & 0, & + \\ 2, & 2, & 0, & + \end{pmatrix}$$

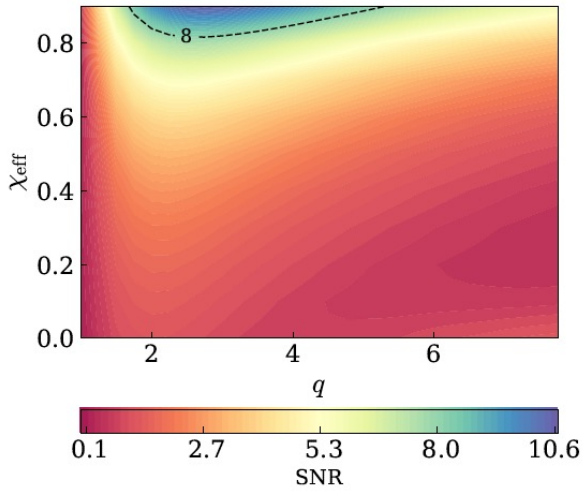


$$\begin{pmatrix} 3, & 3, & 0, & + \\ 2, & -2, & 0, & - \end{pmatrix}$$

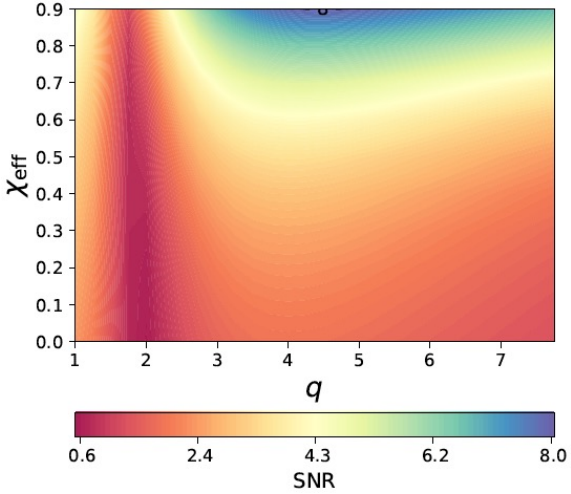


$$\begin{pmatrix} 4, & 4, & 0, & + \\ 2, & -2, & 0, & - \end{pmatrix}$$

- Better approach for multi-signal fitting for BH ringdowns is needed.

# Content

- Classification of linear and nonlinear black hole perturbations.
- Quadratic modes: insights from numerical simulations.
- Quadratic modes: analytical theory.
- Recent progress on QNM tomography.

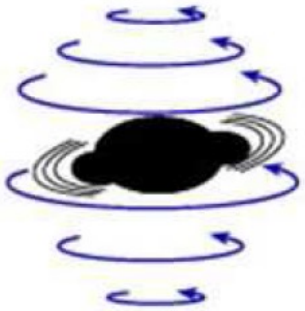

# Black hole tomography

- For the QQNMs we have observed their signatures at infinity and at black hole horizon.

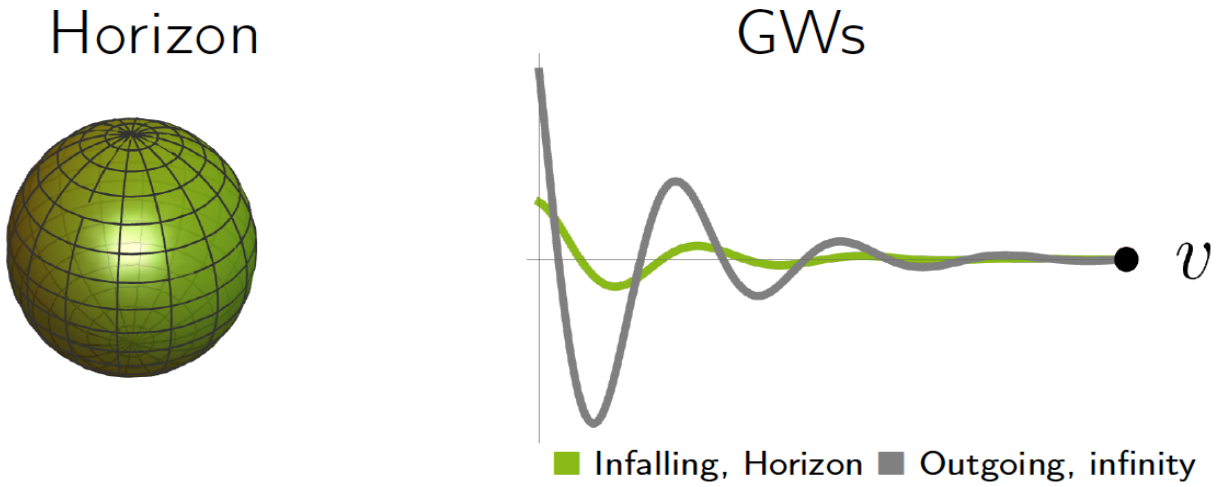


- Interesting to explore the mapping/relation between the two null surfaces, e.g. during the ringdown stage.

# QNM tomography

- Studying the geometry of the horizon can provide insights into the physics of the system at its most strong-field regime..

- Analyzing the ringdown regime can help us distinguish between QNM models and which models are truly present.

- The QNM tomography is well understood in the perturbative regime [e.g. Mitidieri et al.]. We'd like to directly build the connection with the data from numerical simulations.

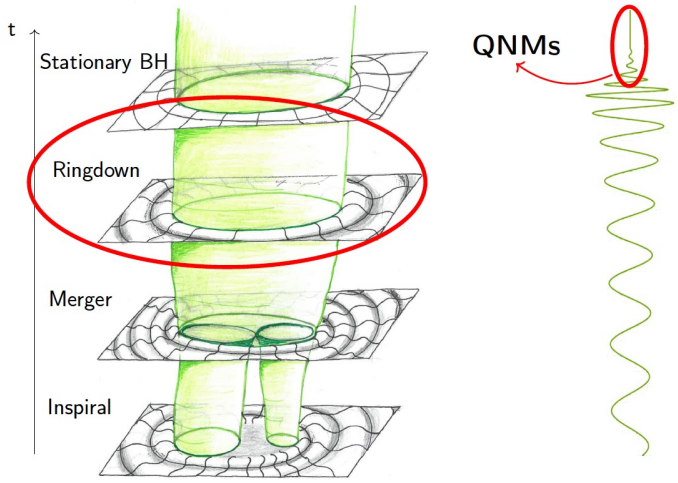

# Quasilocal method to find time $t_{BL}$

- Perturbation theory predicts $I_{lm} \sim A^{H}_{lmn} e^{-i\omega_{lmn} t_{BL}}$. Here $t_{BL}$ is Boyer-Linquist time.
- Numerical simulations give $I_{lm}(t_{NR})$, where $t_{NR}$ is the simulation time. Relating $t_{NR}$ to $t_{BL}$ is a nontrivial task.
- It turn out that, if $g = \frac{\partial t_{NR}}{\partial t_{BL}}$ and it satisfies

$$\left(-\tilde{D}^2 - 2\tilde{\omega}^a \tilde{D}_a - (\tilde{D}_a \tilde{\omega}^a - \tilde{\omega}_a \tilde{\omega}^a + \frac{1}{2}\tilde{R})\right) g = -\kappa_{\circ} \theta_{(\bar{n})}$$

- If $g \approx g_{Kerr} + h$, the solution determined by this PDE is locally equivalent to $t_{BL}$ of $g_{Kerr}$.

- $t_{BL}$ is determined up to $t_{BL} \to t_{BL}$+const by fixing supertranslation on the horizon.

# Comparison of QNM fits with different time

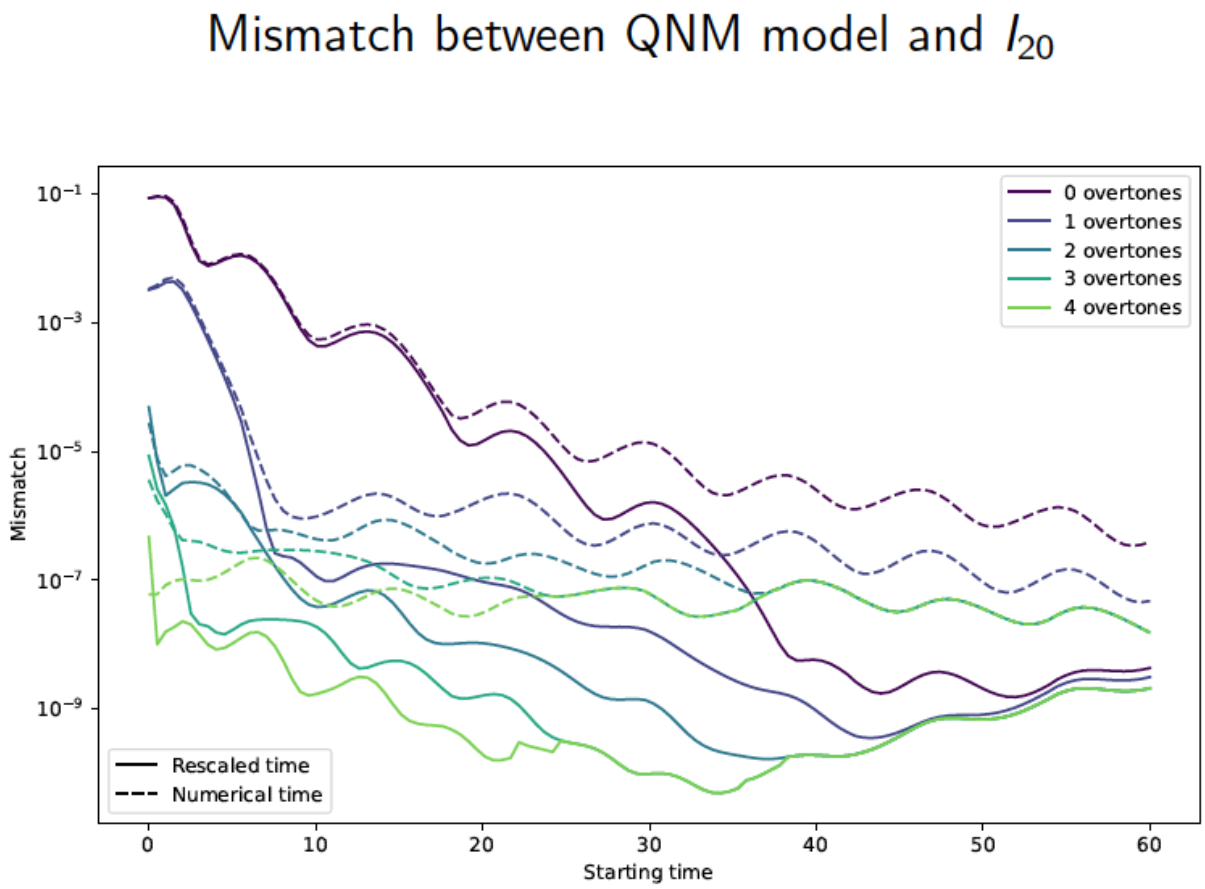


Head-on collisions

# Tomography

- To build the tomography, we first need a mapping between the time on the horizon and v at null infinity.
- For QNMs, the ratio $A^{H}_{lmn}/\ A^{I^+}_{lmn}$ is independent of initial data and a prediction of perturbation theory.
- $A^{I^+}_{lmn}$ can be converted to amplitude of strain at future null infinity and $A^{H}_{lmn}$ can be converted to amplitude of multiple moment.

- By matching the amplitude of the dominant mode, $t_{BL} \rightarrow t_{BL}$+const freedom can be fixed.

# Checking the (2,0,0) mode

Using $\mathcal{A}^{\mathscr{I}^+}_{200}$, we obtain predicted amplitudes of $\mathcal{A}^{\mathcal{H},\mathrm{pred}}_{200}$

$t_{\mathrm{BL}} \to t_{\mathrm{BL}} + \mathrm{const}$ is fixed by $|\mathcal{A}^{\mathcal{H}}_{200}| = |\mathcal{A}^{\mathcal{H},\mathrm{pred}}_{200}|$

Error $\Delta\mathcal{A}^{\mathcal{H}}_{200} = \mathcal{A}^{\mathcal{H}}_{200} - \mathcal{A}^{\mathcal{H},\mathrm{pred}}_{200}$ is only from phase.

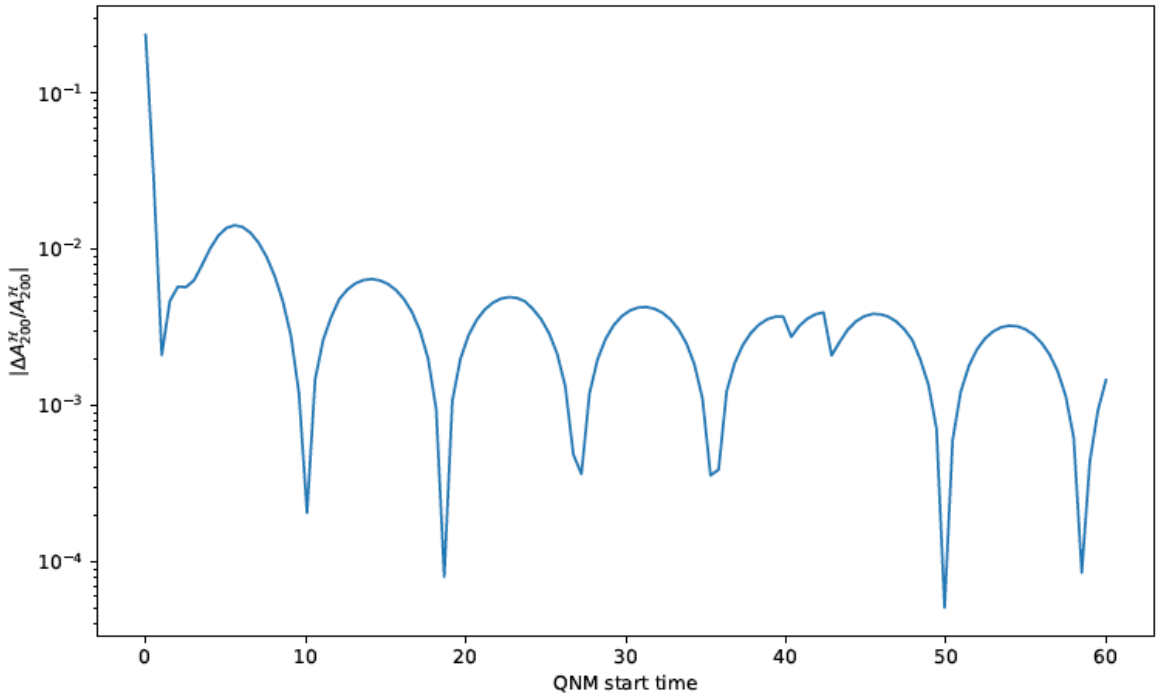


Error is of order $\sim 0.5\%$

# Checking the (2,0,0) mode

Using $\mathcal{A}^{\mathscr{I}^+}_{200}$, we obtain predicted amplitudes of $\mathcal{A}^{\mathcal{H},\mathrm{pred}}_{200}$

$t_{\mathrm{BL}} \to t_{\mathrm{BL}} + \mathrm{const}$ is fixed by $|\mathcal{A}^{\mathcal{H}}_{200}| = |\mathcal{A}^{\mathcal{H},\mathrm{pred}}_{200}|$

Error $\Delta\mathcal{A}^{\mathcal{H}}_{200} = \mathcal{A}^{\mathcal{H}}_{200} - \mathcal{A}^{\mathcal{H},\mathrm{pred}}_{200}$ is only from phase.

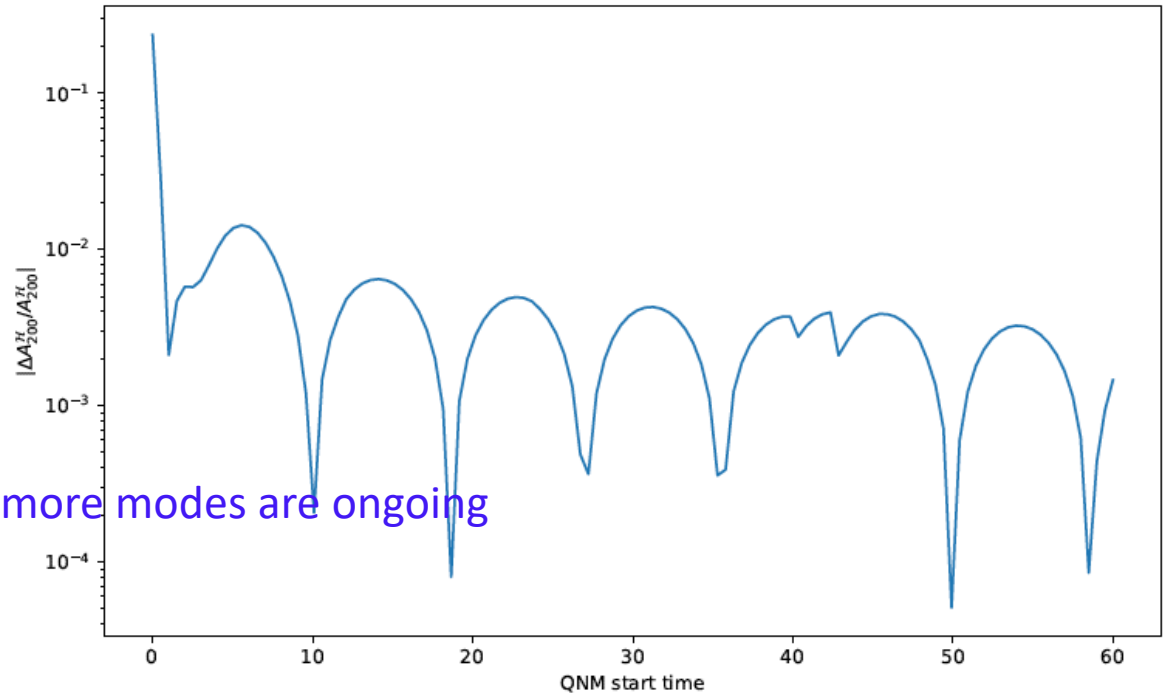


Works on more modes are ongoing

Error is of order $\sim 0.5\%$

# Conclusion

- Past works are mainly focusing on QNM spectroscopy.
- The QQNMs of Kerr can be classified and computed with $2^{nd}$ order Teukolsky equation; good matching with numerical simulations.
- As a community we are starting to understand no-modal part of the GW signal and various non-linear signals, as a way to build better ringdown models.
- QNMs (linear and nonlinear) are useful for black hole tomography.